The Trapeze Instability in an Equatorial β-Plane

ISIDORO ORLANSKI

Geophysical Fluid Dynamics Laboratory/NOAA, Princeton University, Princeton, N.J. 08540

(Manuscript received 2 October 1975, in revised form 23 December 1975)

ABSTRACT

From preliminary reports of the GATE experiment it was concluded that there is some strong evidence that mesoscale waves with a periodicity close to 2 days exist in the equatorial regions. The dynamics of unstable internal gravity waves due to trapeze instability was discussed by means of a two-dimensional, β-plane numerical model. It was concluded that the trapeze instability may be the means by which the observed 2-day waves are excited.

1. Introduction

Since the late 1960's, scientists have shown a considerable amount of interest in trying to explain the rather complicated dynamics of the equatorial region, a region which exhibits fundamental differences from the quasi-geostrophic dynamics of the middle latitudes. Some theoretical studies (Lipps, 1970) have shown that barotropic instability in the easterlies of the equatorial region could be the important source for synoptic waves rather than the baroclinic source that is predominant in middle latitudes. The analysis of observations made in the Pacific by Yanai (1963) have led to the conclusion that easterly waves are present in the equatorial region with periods of about 5 days and wavelengths of 5000 km, and that precipitation patterns are strongly affected or controlled by such waves. These results were confirmed by Reed and Recker (1971), Murakami (1972), Nitta (1972), and others. Prior to these studies, it was independently realized by other scientists that heat release by condensation in the tropics plays an important role as a source of available potential energy for equatorial waves (the CISK mechanism). A complete theoretical study by Yamasaki (1969) shows the role of such energy sources in the easterly waves.

In the process of understanding the dynamics of equatorial waves, a major advance was made when Matsuno (1966) showed that Rossby waves, mixed Rossby waves, inertial gravity waves, and Kelvin waves were capable of coexisting in an equatorial β-plane. All these large-scale waves were identified in the equatorial atmosphere as well as in general circulation models (Hayashi, 1974). However, at present the selection mechanism of these waves is not apparent (Hayashi, 1970; Lindzen, 1974).

One of the purposes of the present paper is to discuss the significance of certain aspects of the above-mentioned observational studies (Murakami, 1972; Nitta, 1972; etc.) which have received little attention in the literature. In particular, the observations we refer to display a periodicity of close to 2 days as shown in precipitation patterns as well as in other meteorological variables in the equatorial region.

Orlanski (1973) has pointed out that the diurnal variability of the static stability of the atmospheric boundary layer could be a major source of internal gravity waves. This source of available potential energy for mesoscale waves could be compared to baroclinicity for large-scale waves in middle latitudes. One of Orlanski's results was that the diurnal variation of the atmospheric static stability is able to excite gravity waves that range from periods of 2 days to a few hours and from horizontal scales of a few hundred kilometers to 1 km. It was also pointed out that the low-frequency waves (with periods of the order of 1–2 days) are highly dependent upon latitude, mainly because internal gravity waves cannot have periods larger than the local inertial period. For instance, the 2-day wave could only extend from 15°N to 15°S and the 1-day wave from 30°N to 30°S.

It was pointed out by McEwan and Robinson (1975) and Thorpe (1975) that the trapeze instability (known as parametric instability in other fields of physics) discussed by Orlanski need not require a stationary oscillatory field like the atmospheric boundary layer, but may be excited even by a large-scale propagating wave. Such an excitation may be the principal mechanism by which energy cascades from large-scale waves to smaller scale waves.

In his analysis of a simple, dry atmospheric model without mean flow, Orlanski found that the most unstable waves in the equatorial region ($f=0$) due to trapeze instability have 2-day periods and about 400 km wavelengths. It is necessary to point out

that, in the case of diurnal forcing, the atmosphere provides a vertical scale (the height of the boundary layer) and that the most unstable waves have periods of twice the forcing period of 1 day. The horizontal scale is therefore determined by the dispersion relation for internal gravity waves. It is apparent that, if these waves are excited in the equatorial area, they will play an important role in the generation and control of mesoscale systems in such regions.

2. Further observational evidence of a 2-day wave

In the last few years large amounts of observational data have been obtained in the tropical region by polar orbiting satellites and by tropical experiments

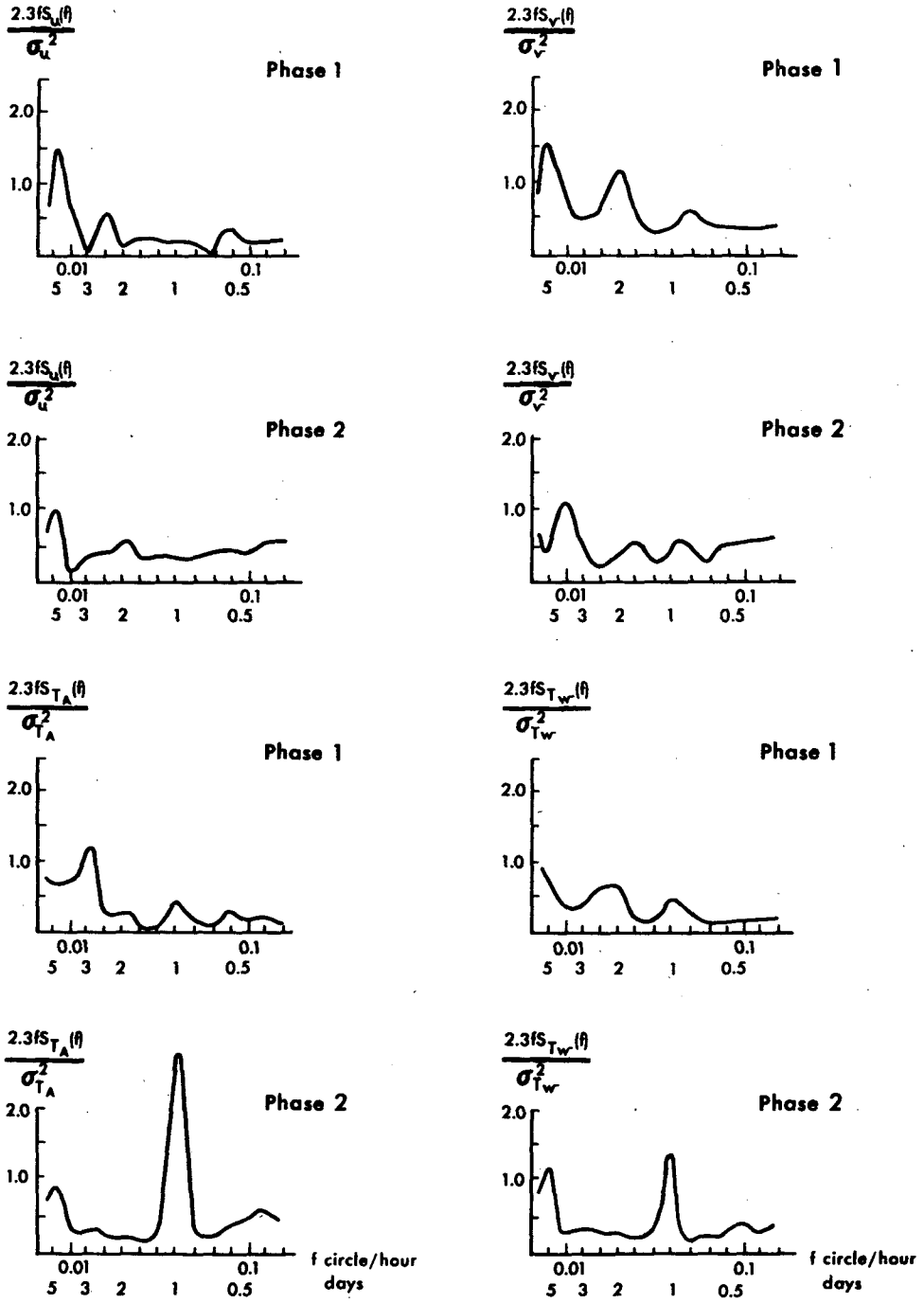

FIG. 1. Density spectra of surface wind u and v, sea-surface temperature T_a and water temperature T_w for phase 1 and 2 in the GATE area (after Petrossiants *et al.*, 1975).

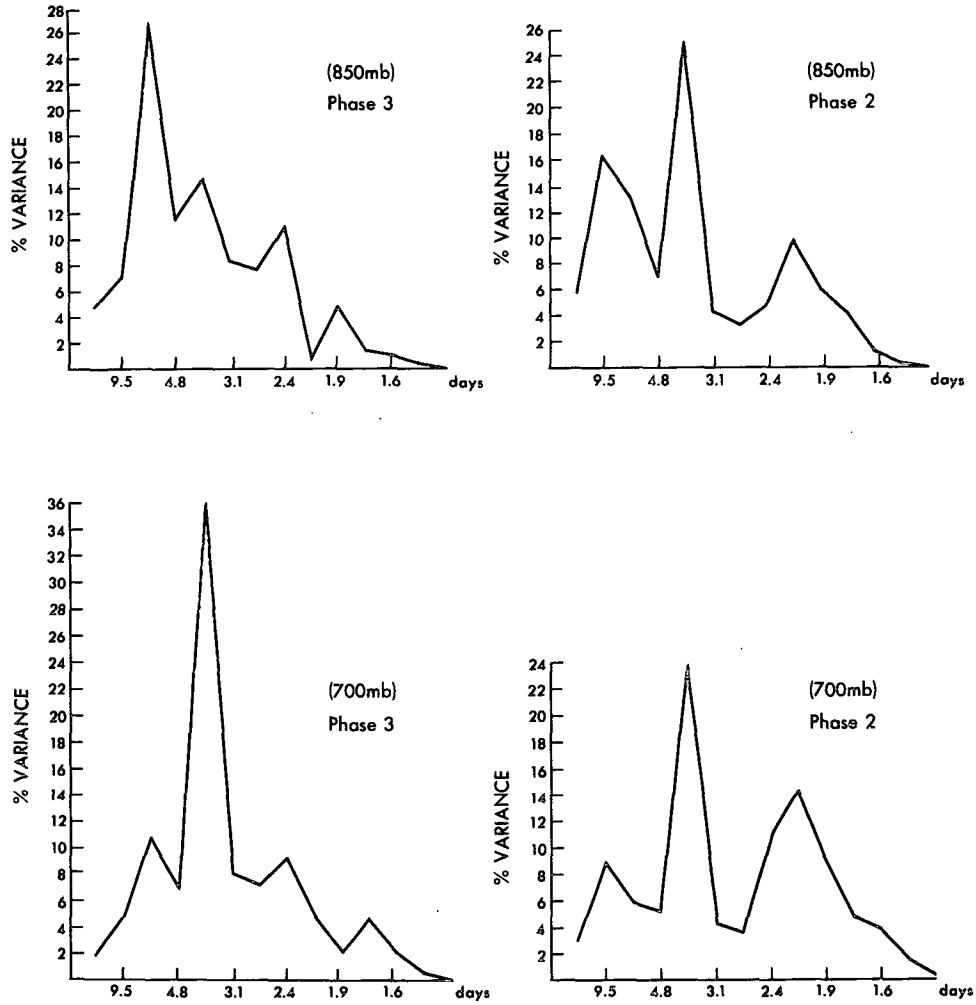

FIG. 2. Spectral analysis of the meridional wind component v at two different heights (850 mb and 700 mb) for phases 2 and 3 of GATE (after Rodenhuis, 1975).

like TROPEX (1972) and BOMEX (1969). The statistics of cloud coverage from such orbital satellites have been inadequate to describe periodicities close to 1 day and unreliable for the 2-day variability. Also, TROPEX and BOMEX were local experiments and were not geared to observe wave dynamics. However, they have provided answers to related important questions. In particular, they have proven that the diurnal variability over the ocean is at least ten times larger than what it was believed to be (Nitta, 1974), although this variability is, of course, smaller than that in the planetary boundary layer over land.

The recent GATE (1974) experiment in the tropical Atlantic provided scientists with a large amount of independent data concerning dynamics of the equatorial atmosphere. In the years to come, we will see the final results of this gigantic experiment. However, some preliminary results are already available.

Fig. 1 shows the density spectra of four meteorological variables, surface wind u and v (upper left and upper right) and sea-surface temperature T_a and water temperature T_w (lower left and lower right) for the GATE area (phase 1 and 2)[1] [after Petrossiants *et al.* (1975)]. Note that, in addition to the 4–5 day peak in the surface wind, there is also a distinct 2-day peak that is most evident in the meridional v component. However, it is not clear in the atmospheric temperature T_a; rather, the diurnal peak is shown to be more predominant, particularly in phase 2. A 2-day peak appears in the water temperature T_w in the period of phase 1; this seems to be correlated with the large peak in the meridional wind v of phase 1. Later in this paper, we will attempt to explain why the 2-day peak is more predominant in the frequency distribution of certain variables.

[1] Phase 1 from 27 June to 16 July 1974, phase 2 from 28 July to 16 August 1974, phase 3 from 30 August to 18 September 1974.

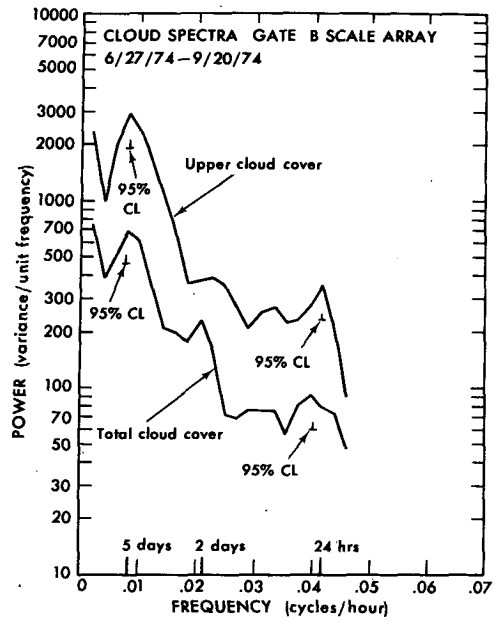

FIG. 3. Spectral analysis of the cloud cover over the B array in the GATE area (after Gruber and Replane, 1975).

The spectral analyses of the meridional wind component at 850 mb and 700 mb for phases 2 and 3 of GATE are shown in Fig. 2. The observations, taken by five ships located along an east–west line at 10°N, were analyzed by Rodenhuis.[2] The general characteristics are similar to those computed by Petrossiants *et al.*; a large peak in the proximity of 5 days and other smaller, but clearly identified peaks around 2 days.

One can argue over the uncertainty of such peaks due to the shortness of the records (each phase involved only 19 days). However, Petrossiants *et al.* computed the cross correlation of water temperature with air temperature and meridional velocity with air temperature, in both cases, and found a significant peak in periods close to 2 days. Only a 5-day peak was found for the cross correlation of u and v.

Further evidence of a 2-day periodicity is found in the fact that the spectral analysis in Fig. 3 made by Gruber and Replane (1975)[3] of the cloud cover over the B array in the GATE area shows a significant peak at this period.

Complimentary results to those of Gruber and Replane (1975) were obtained by Martin (1975) in which the lifetime of cloud clusters in the Atlantic were computed for the three scale arrays, C, B and A/B of GATE, as well as the time of appearance of clusters over Africa and the Atlantic region. The histograms of lifetime and time of appearance are shown in Fig. 4. The lifetime of clusters was found to be: approximately 15–18 h in the C array (3° by 3°), about 24 h in the B array (7° by 7°), and a few days in the larger A/B array. Also, notice that over land (West Africa) the time of cluster appearances is close to 1800 local time (sunset). More evidence of such cloud-cover periodicity can be seen in Fig. 5. This is a composite picture of cloud patterns over Africa in strips of 10° latitude for about 16 days (1–16 November 1974) with night infrared from 1500 to 0300 h in the upper figure, and day infrared from 1000 to 1400 in the lower figure. The strips were presented on alternate days with the purpose that, if a 2-day variability were present, it would be seen more clearly. The right side (even days) of the upper figure shows large compact clusters at 20°E in contrast with the figure on the left (odd days) which is completely clear around 20°E bounded by a small band of clouds on each side. Notice that during the daytime it is more difficult to see any 2-day periodicity. We must comment here that the appearance of intense clouds during early evening is in agreement with Martin's results.

In summary, there is significant evidence of the existence of wave periods close to 2 days in some meteorological variables such as meridional velocity and water temperature and weak evidence in the atmospheric surface temperature data. Also, cloud cover exhibits a significant 2-day peak, while the lifetime of cloud clusters is approximately 1 day for scales of the order of 500 km. Notice that the latter results are consistent with a wave pattern of 2-days period since upward motion in the wave occurs for a half-period, 1 day (the time in which clusters appear), and downward motion for the following half-period (the time in which the clusters are destroyed). A result that we must bear in mind is that, over land (West Africa), cloud clusters appear during the early evening hours.

In the following sections, we will discuss the numerical solution of a two-dimensional, β-plane atmospheric model and will attempt to explain more comprehensively the characteristics deduced from the observational results presented in this section.

3. Mathematical model

In order to understand the dynamics of the observed processes discussed in the previous sections, we will employ a numerical model to extend Orlanski's (1973) conclusions to a more realistic situation involving an equatorial β-plane.

The simplified model used by Orlanski (1973) was partially extended by Fels (1974) considering a semi-infinite domain rather than the assumption of a rigid tropopause made by Orlanski. Rotunno (1975) investigated the effect of a shear flow on the trapeze

[2] Personal communication.

[3] Personal communication (preliminary analysis of GATE cloud and wind data; presented at 9th Technical Conference on Hurricanes and Tropical Meteorology, May 1975, Key Biscayne, Fla.).

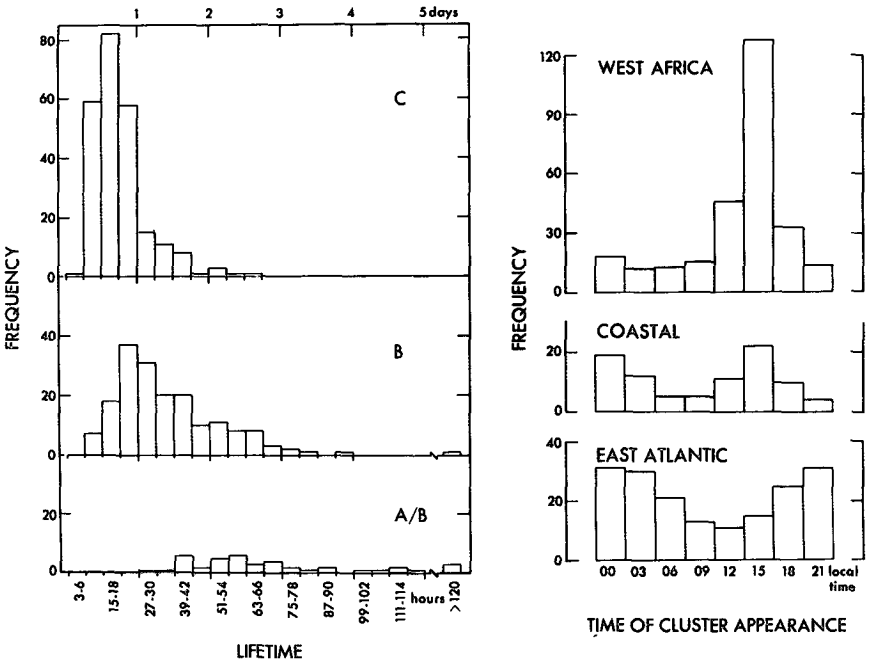

FIG. 4. Frequency of lifetime duration and time of cluster appearance over Africa and the GATE area (after Martin 1975).

mechanism and concluded that the most unstable waves in the presence of strong shear will be two-dimensional rolls parallel to the wind direction. The explanation of this is quite straightforward. Since it is known that a shear flow will modify the frequency of the waves which propagate in the direction of the wind, the resonance condition (i.e., the frequency of the most unstable waves must be half the forcing frequency) will be destroyed for such waves. Hence, shear flow will be a stabilizing effect for these waves. However, for weak shear, the waves will be three-dimensional and isotropic in the horizontal plane.

In the present paper, we will for simplicity consider the case in which only rolls parallel to the mean flow are possible. Thus we may treat the problem as two-dimensional in a vertical-meridional plane. The numerical model to be used is similar to the one described by Orlanski *et al.* (1974) in a study of the dynamics of the atmospheric boundary layer. Specifically, the model was simplified by assuming that the predicted quantities do not depend on one of the horizontal Cartesian coordinates (the east–west component x in the present case). However, in order to incorporate rotational effects, we need to retain the velocity component in the x direction. Since the mesoscale dynamics are assumed to be partially modified by the zonal shear of a large-scale geostrophic flow, a horizontal temperature gradient consistent with the thermal wind relation is included in the north–south direction. We assume that the Coriolis parameter f is a linear function of y ($f=\beta y$). The primitive equations are

$$\frac{\partial \mathbf{V}}{\partial t}+\mathbf{V}\cdot\nabla\mathbf{V}+f\mathbf{k}\times\mathbf{V}=-C_p\theta\nabla\pi-g\mathbf{k}+\frac{1}{\rho_0}\nabla\cdot\tau \tag{3.1}$$

$$\nabla\cdot\rho_0\mathbf{V}=0 \tag{3.2}$$

$$\frac{\partial\theta}{\partial t}+\mathbf{V}\cdot\nabla\theta=\nabla\cdot\mathbf{F}+A(z)[\bar{\theta}_i(z)-\bar{\theta}_i(3000)]\epsilon_D(t). \tag{3.3}$$

Here $\mathbf{V}$ is the three-dimensional velocity vector with components u, v and w in the x, y and z directions, respectively; $\mathbf{k}$ is the unit vector in the z direction; ρ_0 the mean density (a known function of z); and θ, the potential temperature, is defined as

$$\theta=T(P/P_s)^{-R/C_p},\quad \pi=(P/P_s)^{R/C_p}.$$

$A(z)$ is a coefficient for the forcing term that drives the mean potential temperature to oscillate diurnally in the boundary layer, and is defined as

$$A(z)=\begin{cases}1.0, & 0\leqslant z\leqslant 3\text{ km}\\ 0.0, & 3\text{ km}<z\end{cases} \tag{3.4}$$

and $\bar{\theta}_i$ is the mean initial potential temperature. τ and $\mathbf{F}$ represent the turbulent momentum-stress tensor and turbulent heat-flux vector, respectively. Using the previous assumptions, we can simplify all these equations in the following manner using the streamfunction ψ and vorticity ζ for motion in the

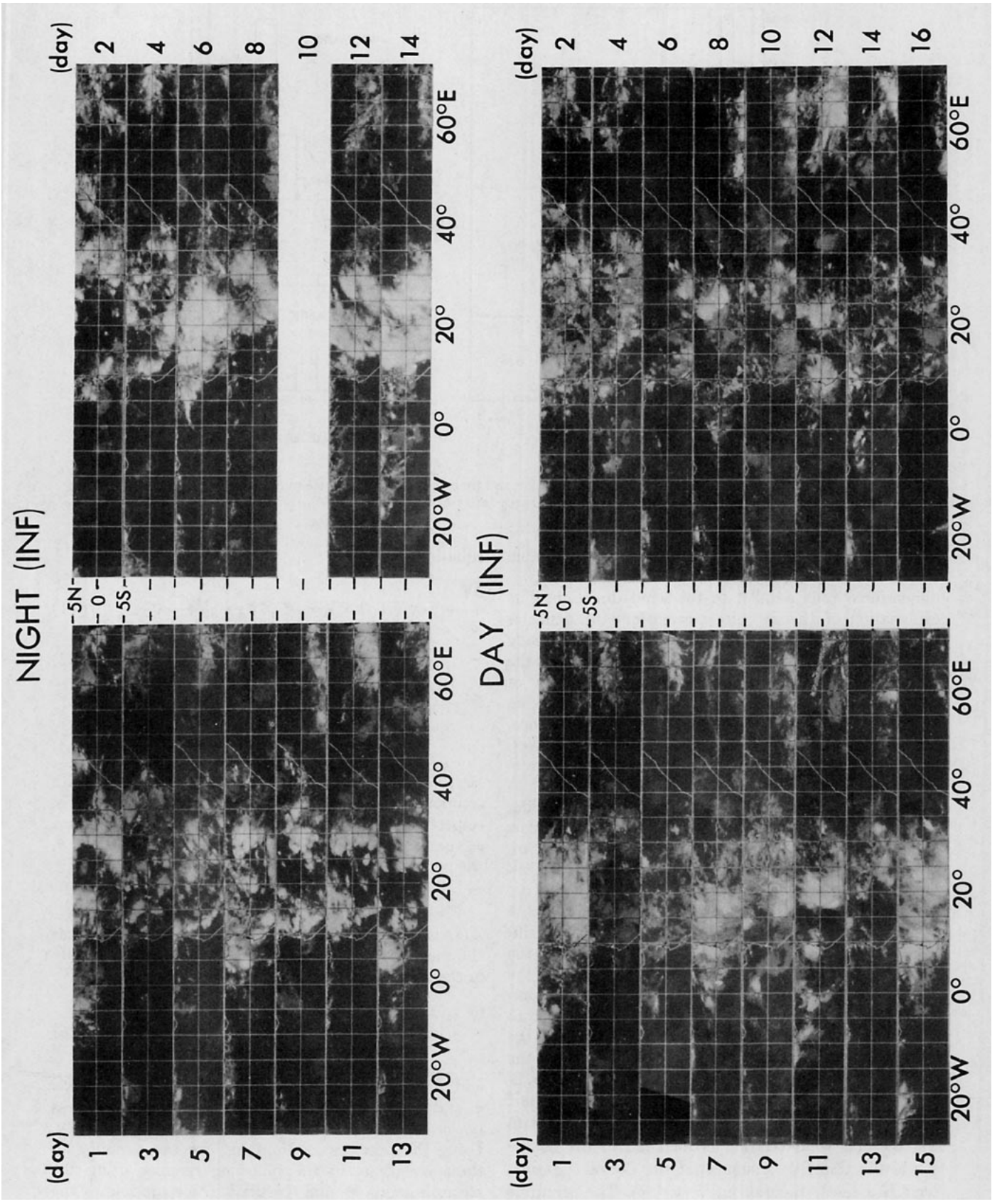
NIGHT (INF)
DAY (INF)
(day)
1
3
5
7
9
11
13
2
4
6
8
10
12
14
15
16
5N
0
5S
20°W
0°
20°
40°
60°E

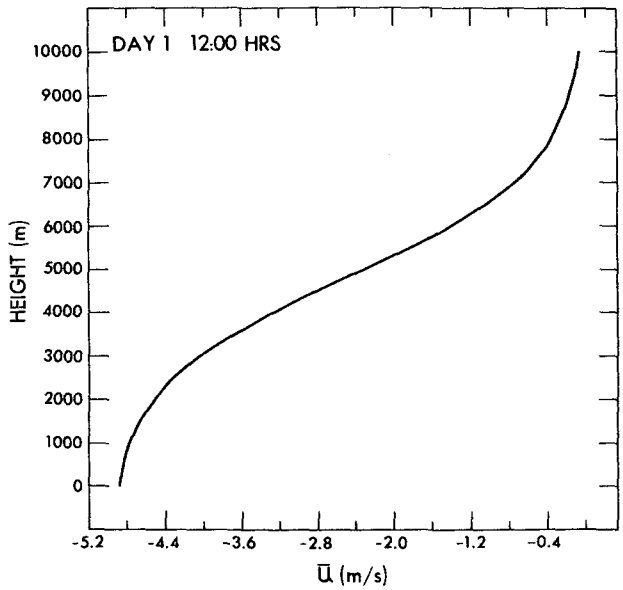

FIG. 6. Vertical profile of the initial easterly mean flow.

(y,z) plane:

$$\frac{\partial \zeta}{\partial t} - J(\psi,\alpha_0\zeta) + fu_z = \frac{g}{\theta_s}\frac{\partial \theta}{\partial y} + \nabla\cdot\nu_e\nabla\xi, \tag{3.5}$$

$$\frac{\partial u}{\partial t} - J(\psi,u) - fv = \nabla\cdot\nu_e\nabla u, \tag{3.6}$$

$$\zeta = \frac{\partial}{\partial y}\left(\alpha_0\frac{\partial \psi}{\partial y}\right) + \frac{\partial}{\partial z}\left(\alpha_0\frac{\partial \psi}{\partial z}\right), \tag{3.7}$$

$$\frac{\partial \theta}{\partial t} - \alpha_0 J(\psi,\theta) = \nabla\cdot\chi_e\nabla\theta + A[\bar{\theta}_i(z) - \bar{\theta}_i(3000)]\epsilon_D(t), \tag{3.8}$$

where

$$\alpha_0 = -1/\rho_0 = \alpha_s\left(1 - \frac{g}{C_p\theta_s}\right)^{-[(C_p/C_v)-1]},$$

and

$$\epsilon_D = \omega_0\epsilon_{0D}\cos\omega_0 T,$$

where ω_0 is the diurnal frequency and ψ is defined such that $\partial\psi/\partial z = v/\alpha_0$ and $\partial\psi/\partial y = -w/\alpha_0$. Notice also that the advective terms have been manipulated such that they are in Jacobian form for the sake of numerical consideration. The turbulent momentum and heat fluxes have been parameterized using eddy diffusivity coefficients ν_e and χ_e which are defined as

$$\chi_e = \begin{cases} \chi_0\left[1 + e\left(-\dfrac{g\Delta\theta(\Delta z)^3}{\theta\chi_0\nu_0}\right)\right]^{\frac{1}{3}}, & \text{if } \Delta\theta < 0 \\ \chi_0, & \text{if } \Delta\theta \geqslant 0 \end{cases} \tag{3.9}$$

where χ_0 and ν_0 are constant background values of eddy diffusivity and viscosity, and Δz and $\Delta\theta$ are local values of the vertical grid size and the vertical difference in potential temperature between grid points. The eddy viscosity ν_e was assumed to be proportional to χ_e with the proportionality constant equal to 1. For more details of the numerical model and the physical constants, we refer the reader to Orlanski *et al.* (1974).

The model has 50 layers in the vertical from the ground to a fictitious tropopause at 10 km with a constant increment Δz of 200 m. In the meridional plane, it extends from 22.5°N to 22.5°S with a constant grid spacing of about 65 km. Rigid wall boundary conditions were applied to the lower boundary; however, open boundary conditions [a radiation wave condition described by Orlanski (1976)] were applied to the north and south boundaries and, in modified form, at the tropopause.

Fig. 6 shows the profile of the initial easterly wind that was assumed constant in the north–south direction. The temperature profile with the diurnal variation in the lower-boundary layer is shown in Fig. 7. The model was initially disturbed with random noise in the temperature field to excite the unstable waves.

In the following sections a discussion of the characteristics of the unstable waves will be presented. This includes the solution for dry atmosphere in Section 4 and the modification due to moisture in Section 5.

4. Trapeze instability (dry atmosphere)

Before discussing the actual numerical solution, we will first review part of the analytic studies made by Orlanski (1973) for small-amplitude unstable waves.

In the case of a dry atmospheric oscillatory boundary layer, a first approximation of Eqs. (3.1)–(3.5) gives

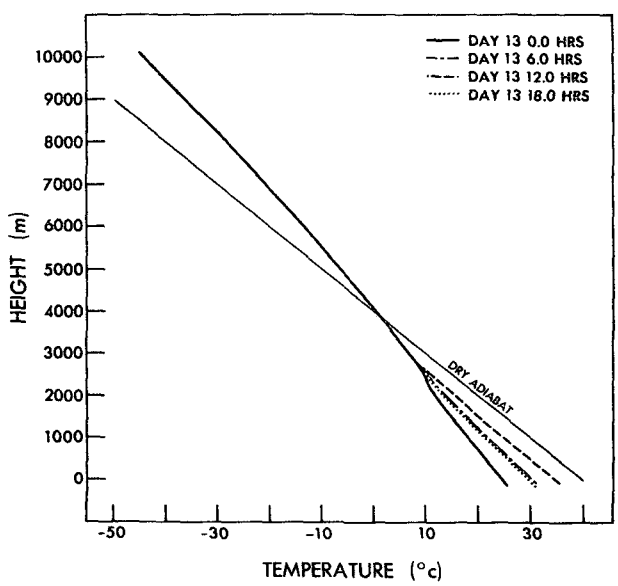

FIG. 7. Vertical profile of temperature showing the diurnal variability of the temperature from the surface to 3000 m.

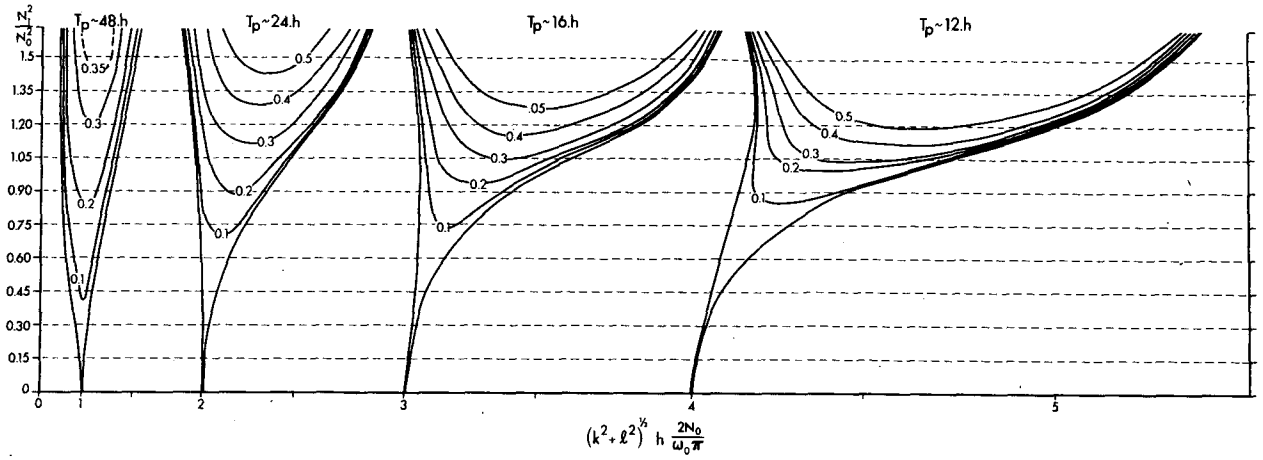

FIG. 8. Contours of the nondimensional growth rate, $\mu=2\nu/\omega_0$, as a function of the nondimensional horizontal scale and the ratio N_1^2/N_0^2. The predominant oscillatory period in the different branches is indicated as T_p.

the following differential equation for the vertical velocity:

$$W_{ttzz}+f^2W_{zz}+\nabla_H^2[W_{tt}+N^2(z,t)W]=0, \quad (4.1)$$

where $N^2(z,t)$ is the square of the Brunt-Väisälä frequency $[+(gd\bar{\theta}/\theta_s dz)]^{\frac{1}{2}}$. Now if the static stability of the boundary layer has a diurnal oscillation, we can define N^2 as $N^2=N_0^2+N_1^2\cos\omega_0 t$, where $N_0^2+N_1^2=N_{\text{night}}^2$ and $N_0^2-N_1^2=N_{\text{day}}^2$. For the simple case in which N_0^2 and N_1^2 are constant with height, the amplitude of the vertical velocity satisfies the differential equation

$$W_{0tt}+\left[\frac{(k^2+l^2)N_0^2+(m\pi/h)^2f^2}{k^2+l^2+(m\pi/h)^2}+\frac{(k^2+l^2)N_1^2}{k^2+l^2+(m\pi/h)^2}\cos\omega_0 t\right]W_0=0, \quad (4.2)$$

provided that

$$w=w_0\sin\left(\frac{m\pi}{h}z\right)e^{i(kx+ly)},$$

where h is the height of the boundary layer, k the vertical wavenumber, and l and m are the horizontal wavenumbers in the x and y directions, respectively. Eq. (4.2) is a Mathieu equation where a general solution for the amplitude ω_0 is

$$W_0\equiv C_1e^{\nu t}\phi(\alpha t)+C_2e^{-\nu t}\phi(-\alpha t), \quad (4.3)$$

where ϕ is a periodic function of the variable $\alpha t=2t/\omega_0$, and ν is the growth rate that depends on the parameters N_0^2, N_1^2, k, l, etc. For the particular case in which $f=0$, Fig. 8 shows the contours of the nondimensional growth rate $\mu=2\nu/\omega_0$ as a function of the nondimensional horizontal scale $(k^2+l^2)^{\frac{1}{2}}h[2N_0/(\omega_0\pi)]$ and the ratio N_1^2/N_0^2. The different branches correspond to distinct oscillation periods of the function $\phi(\alpha t)$. The first branch is approximately a 2-day period, the second a 1-day period, and so on. The characteristic period of the nth branch is $T_n=2$ days$/n$.

As can be seen, the most unstable waves for $N_1^2/N_0^2<1$ correspond to the first branch. We can calculate numerical solutions for different values of N_1^2/N_0^2. However, only one will be discussed here, namely the one corresponding to $N_1^2/N_0^2=0.8$, which is characteristic of equatorial boundary layers. The horizontal scale is determined by the height of the boundary layer since the dispersion relation for the frequency is

$$\omega=\frac{(k^2+l^2)^{\frac{1}{2}}N_0}{[k^2+l^2+(m\pi/h)^2]^{\frac{1}{2}}}. \quad (4.4)$$

For the maximum unstable waves, $\omega=\pi/T_0=\omega_0/2$, and if k and l are very small compared to $2\pi/h$, Eq. (4.4) becomes, for the deepest wave ($m=1$):

$$(k^2+l^2)^{\frac{1}{2}}=\lambda=\frac{2\pi^2}{T_0N_0h}.$$

The inverse horizontal scale λ is then $\sim 2\times10^{-2}\ h^{-1}$. If $N_0\approx(1/86)$ s^{-1} and $T_0=86\times10^3$ s, and for a boundary layer of 3 km height, the horizontal wavelength $L=2\pi/\lambda$ is the order of 900 km.

The time histories of the numerical solution at three different heights (1000, 2000, 4000 m) for the disturbance u, v, w and T at different latitudes (0°, 11°, 17°) are shown in Figs. 9–11. Fig. 9 shows the solutions at the equator. Along the abscissa is the time in days, and the different heights are shown on the left. On the right are the magnitudes of the variability of each record. In the temperature record, the two lower areas inside the boundary layer show a very regular, diurnal periodicity that was forced by the Newtonian cooling term of Eq. (3.3). However, at 4000 m the record is more irregular, and after

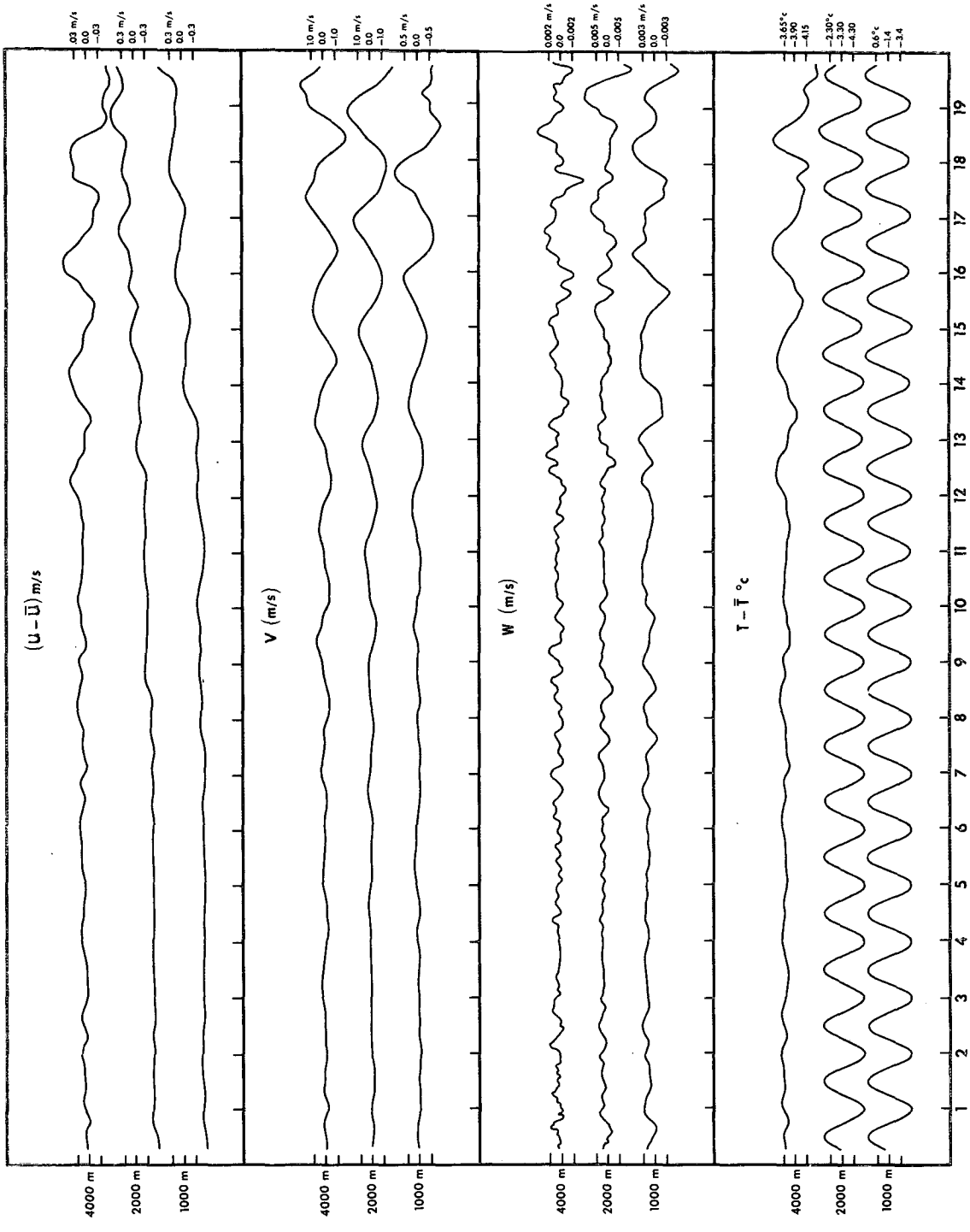

FIG. 9. Time record of u, v, w, and temperature for three different heights (4000, 2000 and 1000 m) given by the numerical model at the equator.

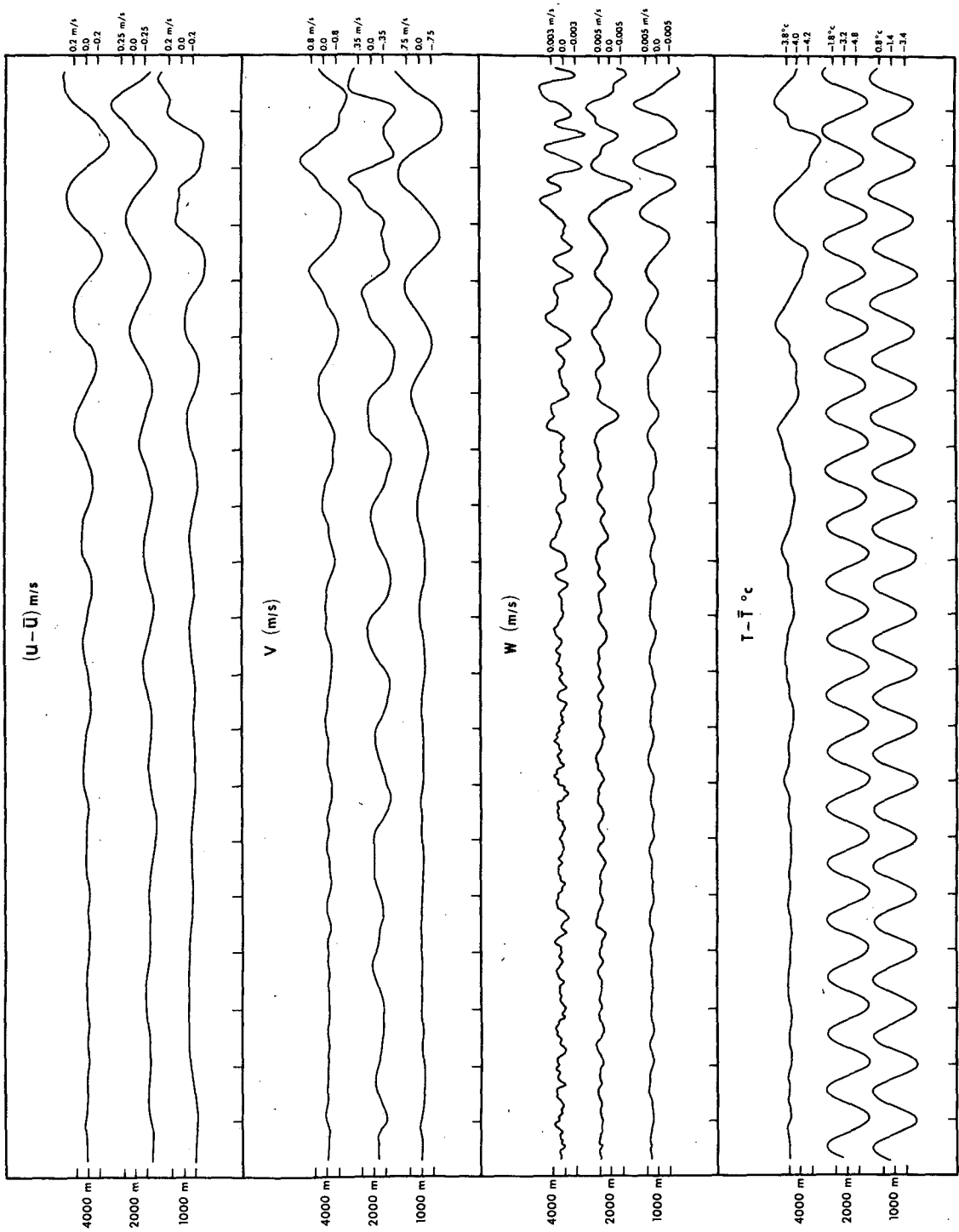

FIG. 10. As in Fig. 9 except at 11.5°N latitude.

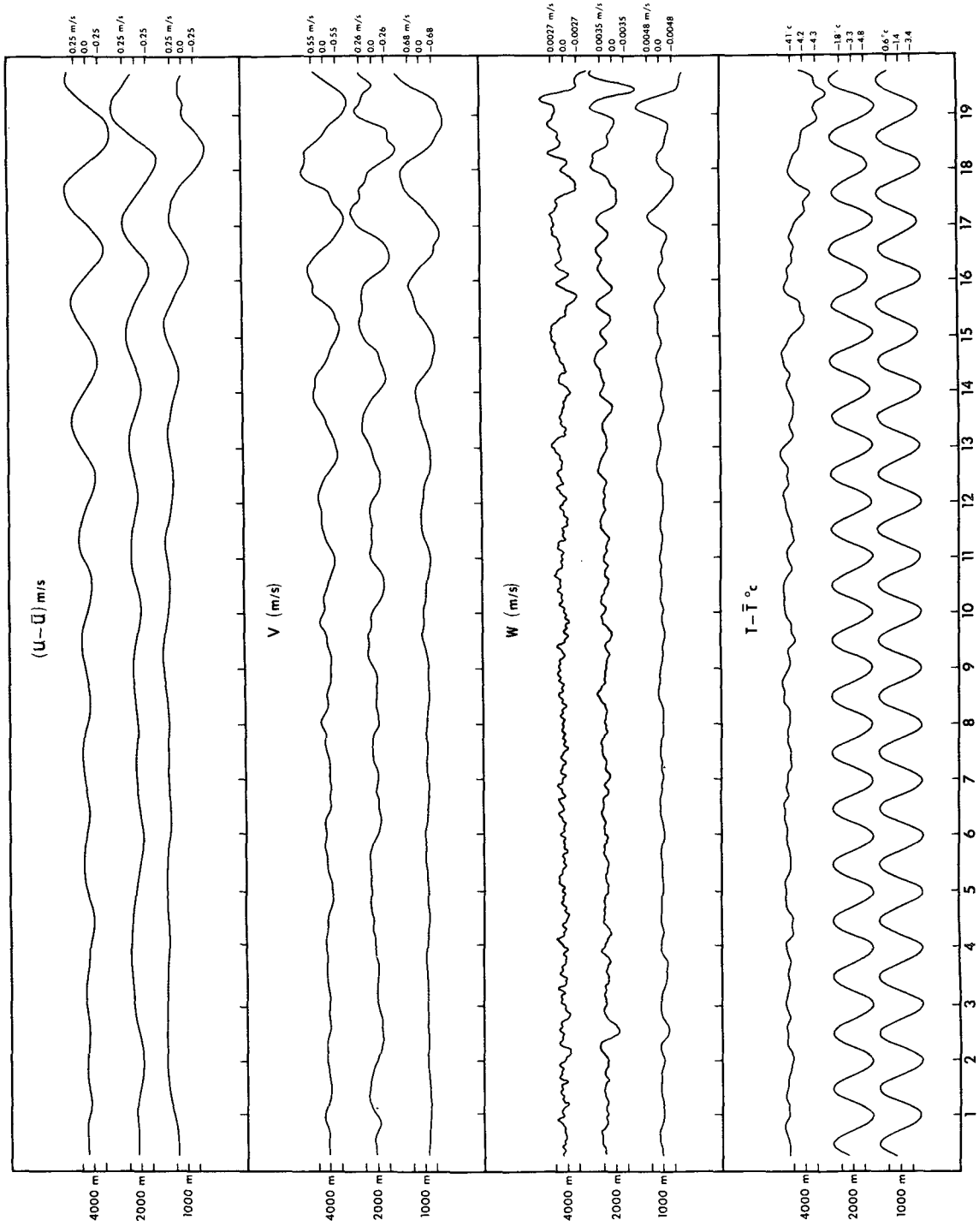

FIG. 11. As in Fig. 9 except at 17°N latitude.

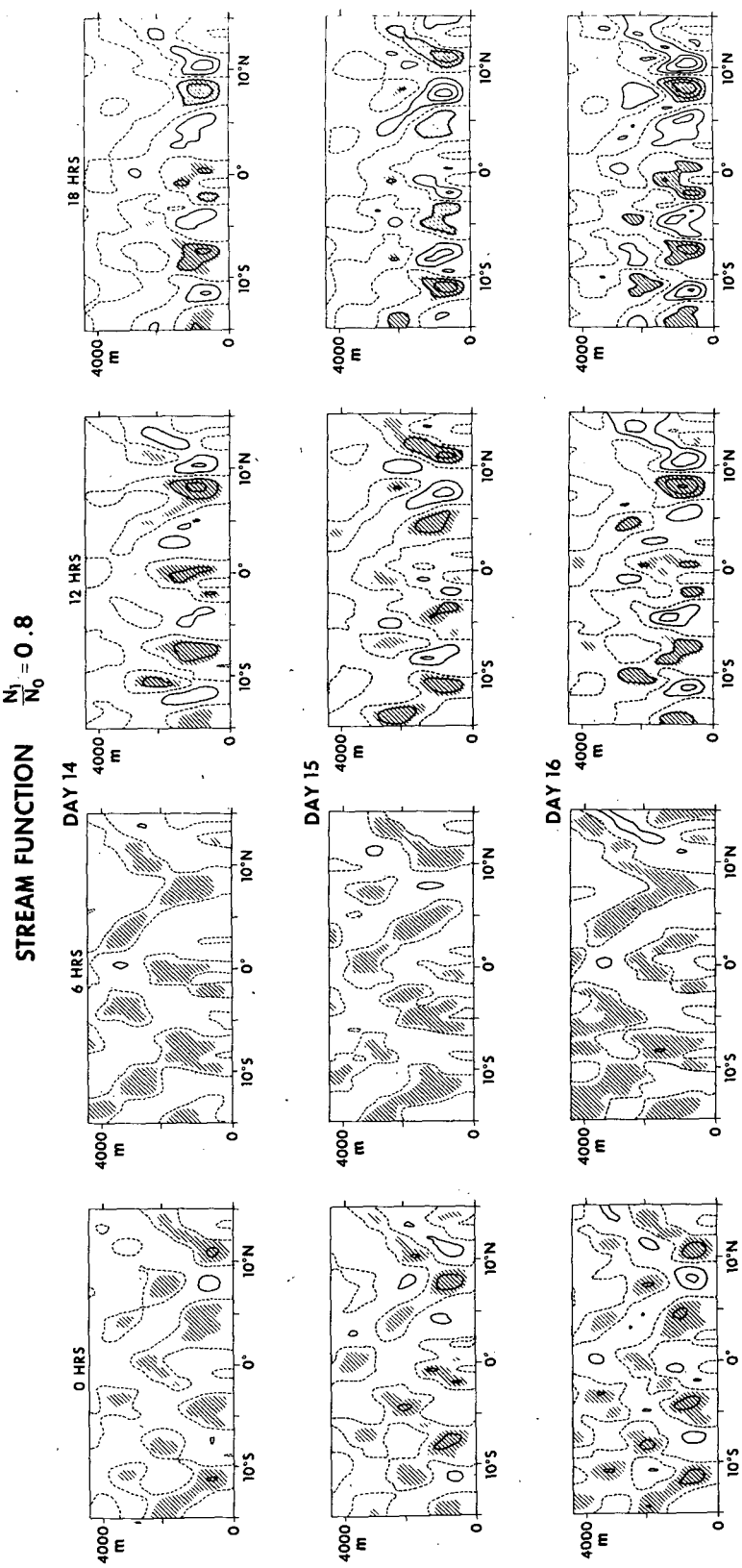

FIG. 12. Contours of streamfunction as a function of latitude and height corresponding to four different times of the day for three consecutive days.

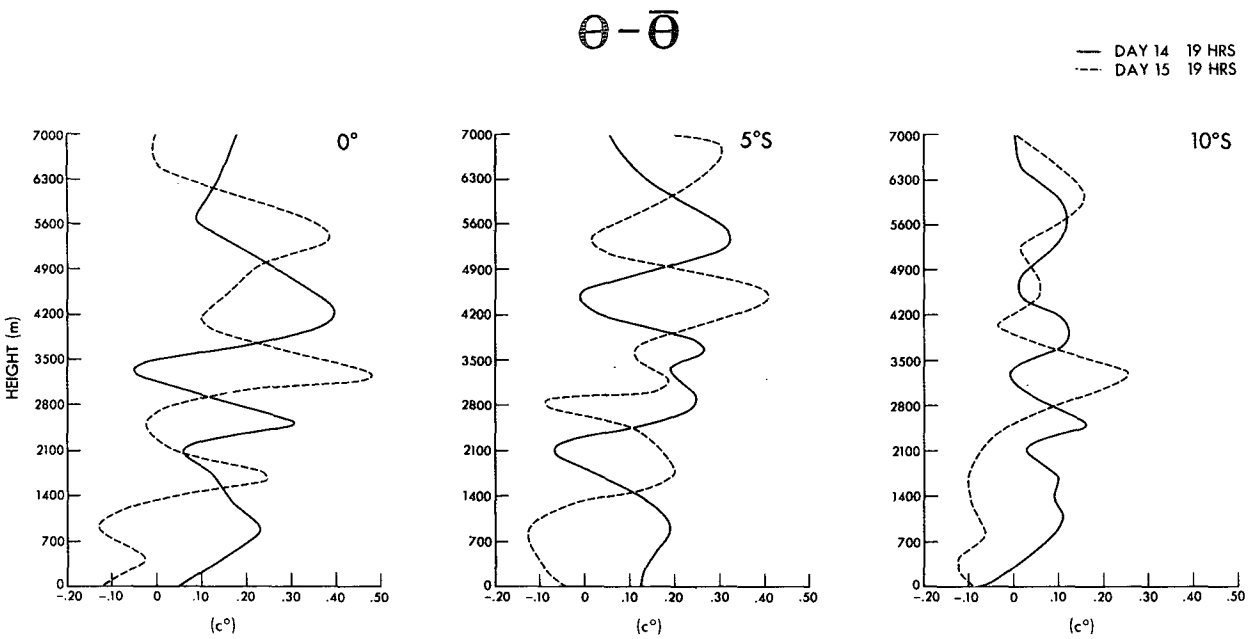

FIG. 13. Vertical profile of the disturbance potential temperature at three different latitudes (0, 5°S, 10°S) for two consecutive days at sunset.

11 days a distinct 2-day periodicity can be observed. This is more apparent in the other variables, particularly at all levels of the meridional wind component v (maximum oscillation of the order of 1 m s^{-1}) but with a smaller oscillation in u and w for this latitude. At 11.5° latitude (Fig. 10), the general behavior is similar to that at the equator; however, the magnitude of the variability of u is increased considerably. The same tendency is observed at 17° latitude (Fig. 11). In this figure, however, the meridional wind variability (v) decreases to half the value at the equator.

A clear understanding of the latitudinal variability of the meridional circulation can be realized by inspecting Fig. 12. In this figure the contours of streamfunction are shown at four times of the day (0000, 0600, 1200, 1800) for three consecutive days when the wave becomes large. The first thing to notice is that the wave activity is minimum at sunrise (0600) and maximum at sunset (1800); this result will be discussed later as a basis for the energy arguments.

Second, the vertical extension is about 2000 m and the approximate horizontal wavelength is 700 km. The maximum circulation is concentrated at approximately 10°N and 10°S. An approximate analytic expression could be found for these solutions by expanding the set of equations (3.5)–(3.8) in their linearized form and then assuming that N_1^2/N_0^2 is very small; the first-order solutions in such an expansion are Hermite-type solutions, similar to those found by Matsuno (1966) for the inertial-gravity modes. Also, notice the alternate pattern of 2-day periodicity that can be seen from the solution, in particular, at 1800. We also point out that the upward motion is located at one latitude on one day and at a half-wavelength away on the next day. For example, at day 15, the maximum upward motion was at 10°N and downward motion at 7°N, while on the following day the reverse situation appears. This effect will be relevant to the discussion of cloud clusters generated by the unstable wave mechanism and will be discussed further in the next section.

The vertical structure of these waves for two consecutive days (days 14 and 15) at the maximum amplitude (at 1900) can be seen in Figs. 13–16 for T, u, v and w, respectively. The profiles were taken at three different latitudes (0°, 5°S, 10°S). The most relevant feature is the 180° phase difference between the solution at these two consecutive days. The vertical wavelength could be estimated to be approximately 2000 m, and although a large decrease in the amplitude is observed above the oscillatory boundary layer at 3000 m, some wave propagation above the boundary layer is noticeable. The largest disturbances by far occur in the wind component perpendicular to the mean flow (Fig. 15). Notice that the magnitude of the vertical velocity is fairly small, reaching no more than 1.5 cm s^{-1} (Fig. 16). We must remember that these calculations are for a dry atmosphere and that the inclusion of moisture will increase this value of w by at least an order of magnitude. In addition, a more realistic value for the ratio N_1^2/N_0^2 is close to 1 over land, thereby making the system far more unstable. However, over the ocean this ratio is closer to 0.5. In any event, this latter case is unstable but weaker than the one previously discussed.

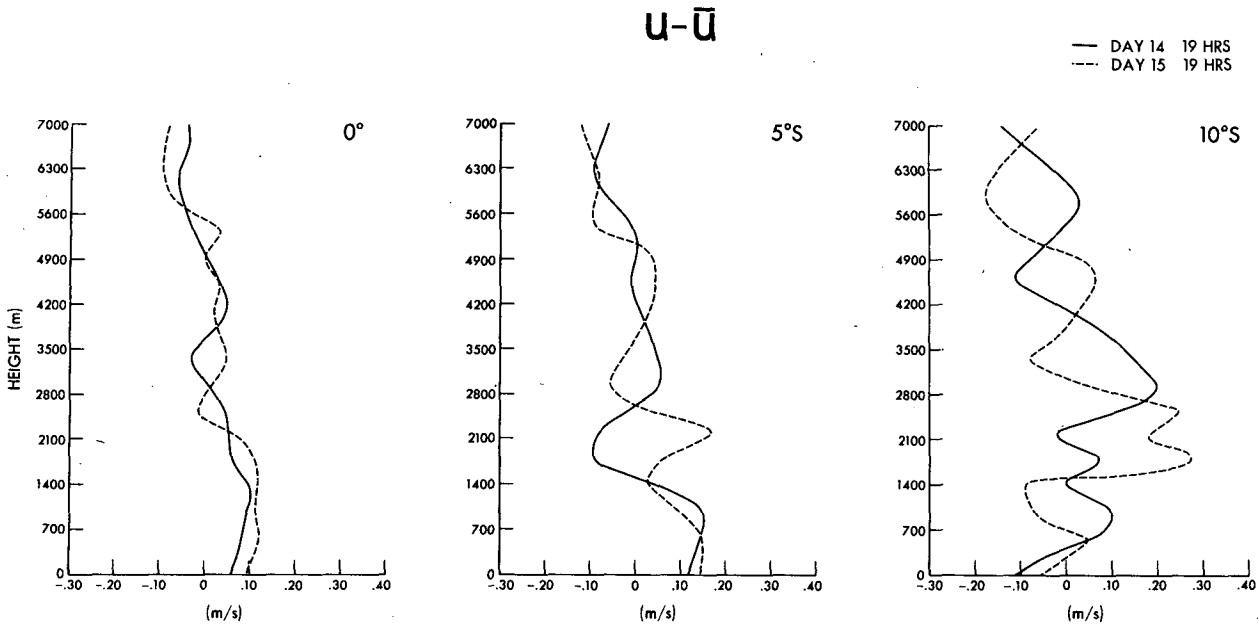

FIG. 14. As in Fig. 13 except for horizontal velocity u.

Before finishing this section, we must consider why the maximum amplitude of the unstable waves occurs at sunset (over land). Orlanski (1973) shows that the energy source for trapeze waves is due to the time variability of the potential energy of the atmosphere. In this regard, he derived the energy balance equation as follows:

$$\int_0^h (\bar{K}+\bar{P})_t = -C_p\theta_0\rho_0(w\pi)_{z=h} - \int_0^h \left(\frac{1}{2}\frac{\rho_0 g\theta^2}{\theta_0(\bar{\theta}_z)^2}\right)\bar{\theta}_{zt}dz. \quad (4.6)$$

The left-hand term is the time variation of the total wave energy in the boundary layer

$$\bar{K}=\rho_0\frac{V^2}{2} \quad \text{and} \quad \bar{P}=-\frac{1}{2}\frac{\rho_0 g\bar{\theta}^2}{\theta_0\theta_z}.$$

The first term on the right-hand side is the work done by pressure force at the top of the boundary layer, and the second term is the source of potential energy that drives the trapeze instability. All the terms in the integrand are positive, excluding the term θ_{zt} which is oscillatory. When this term is positive, the wave loses energy, and conversely, when it is negative, the wave gains energy. Let us see then when the maximum positive and maximum negative values occur. $\bar{\theta}_z$ is minimum at noon hours and maxi-

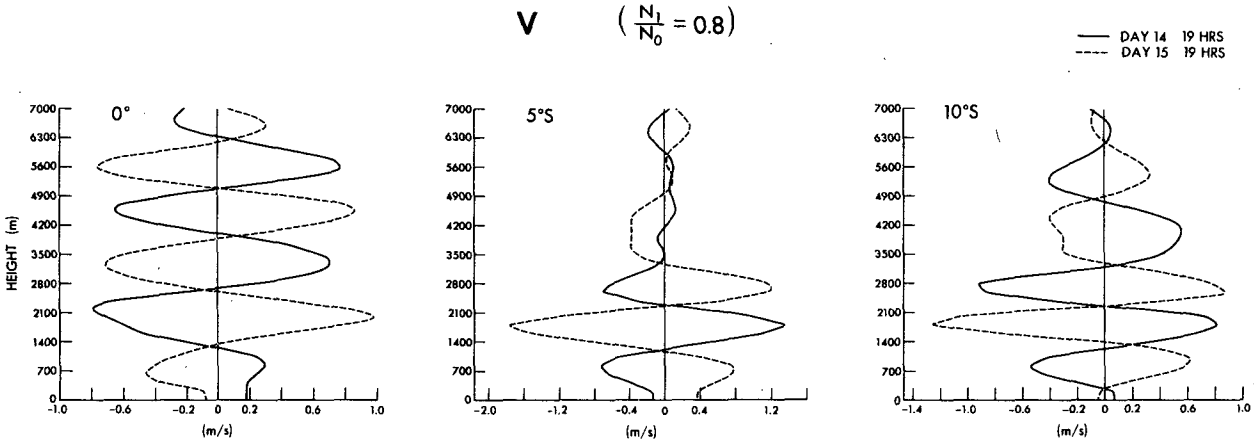

FIG. 15. As in Fig. 13 except for meridional velocity v.

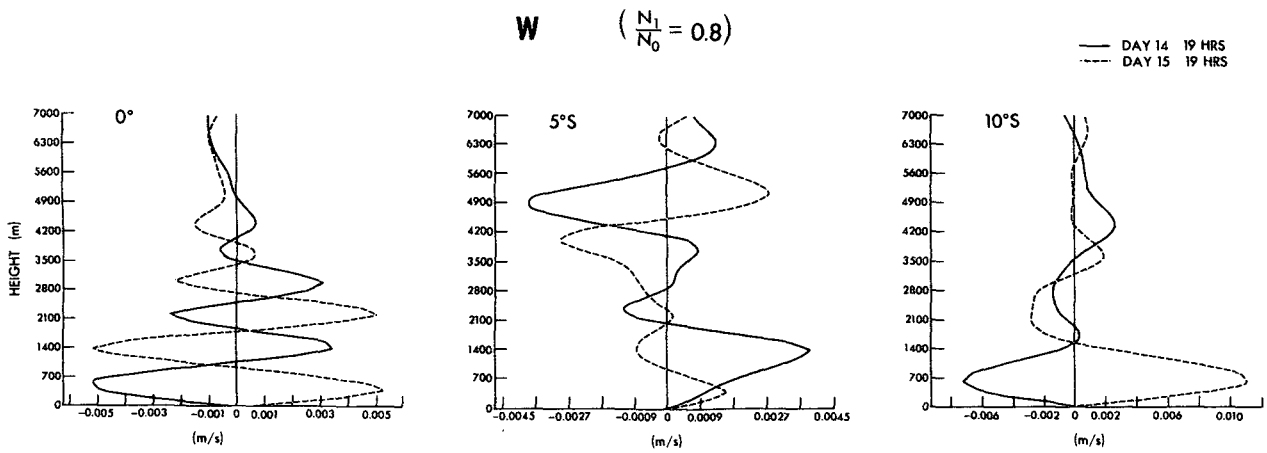

FIG. 16. As in Fig. 13 except for vertical velocity w.

mum at nighttime (at least in the boundary layer over land). Then the source term on the right side of (4.6) will have nodal points at noon and midnight, times at which the total wave energy will have maxima and minima. Fig. 17 shows the time evolution of $(K_e)_t$, $(P_e)_t$, and minus the source term from (4.6) over one full day. It can be seen that $(P_e)_t$ approximately balances the source term. The difference between these two terms is partially balanced by the time-rate of kinetic energy $(K_e)_t$ and by the flux of energy through the top of the boundary layer $(-C_p\theta_0\rho_0\overline{w\pi})$. Notice that the potential energy has extremes at 1200 and 2200 and the kinetic energy, by contrast, has its extremes at 0600 and 1800.

In fact, the evolution in time of the potential and kinetic energy contained in the boundary layer (P_e and K_e) can be seen in Fig. 18, where the diurnal variation of P_e and K_e are clearly noticeable. The maximum and minimum kinetic energy occurs at 1800 and 0600, respectively, whereas the potential energy has a maximum at 1200 and a minimum at about 2200.

The behavior of K_e and P_e are simply explained by the linearized Mathieu solutions of (4.2) where the predominant term of the most unstable solution, corresponding to the first branch of Fig. 8, is $w \approx e^{\nu t} \times \sin[(\omega_0/2)(t-0600)]$ if the diurnal variation of the mean stratification is $\bar{\theta}_x = \bar{\theta}_{0z} - \theta_{1z}\sin[\omega_0(t-0600)]$. Then the most unstable wave will have maximum activity at 1800 and minimum activity at 0600. However, since the potential energy is inversely proportional to the mean stratification, it will have maxima and minima when the mean stratification has minima and maxima.

It is interesting to point out that the estimated nondimensional growth rate $2\nu/\omega_0$ from the numerical solution is about 0.175 where the linear solution from Fig. 8 estimates about 0.2. We must emphasize, however, that the previous discussion of the maximum and minimum are only true as long as the boundary layer is over land where maximum solar heating occurs during daytime and maximum radiational cooling is at night. The diurnal variability over the ocean

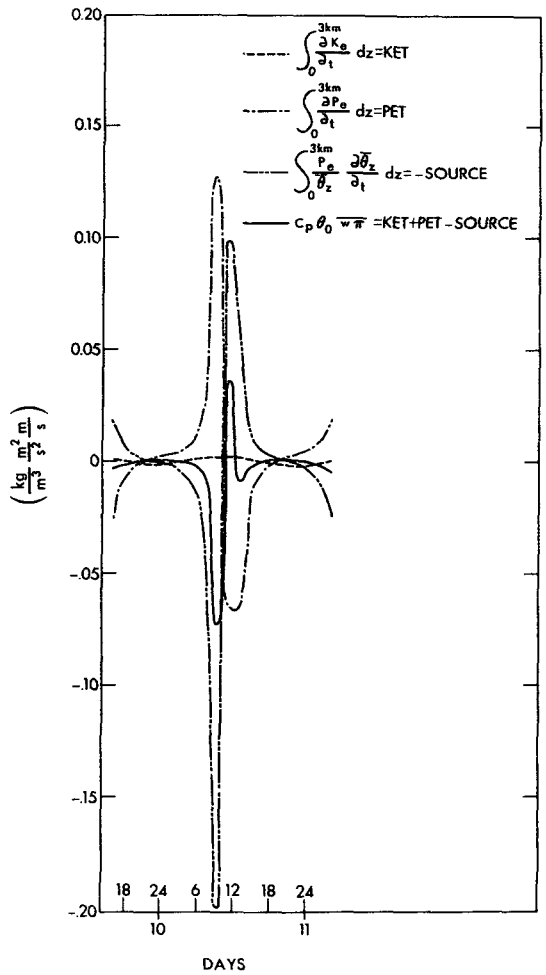

FIG. 17. The time rate of P_e, K_e minus the source term, and the energy flux through the top of the boundary layer over a period of one day.

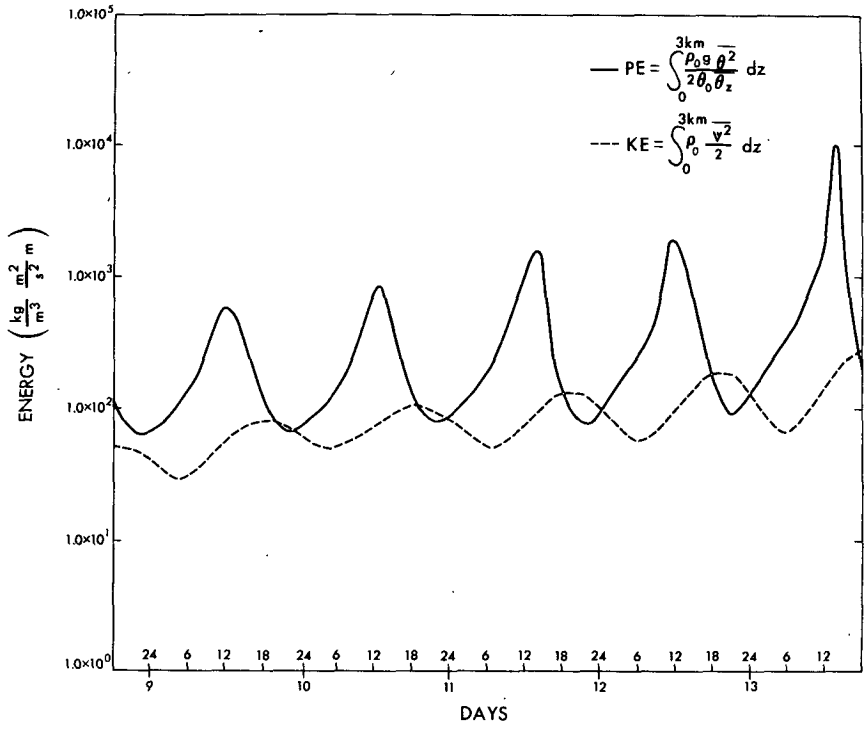

FIG. 18. The integrated potential energy and kinetic energy over the boundary layer as a function of time.

could have different characteristics, and furthermore, the maximum and minimum times may not necessarily correlate with the previous estimations made over land.

In the next section we will discuss the role of moisture in the intensification of these waves.

5. Trapeze instability (moist atmosphere)

The mesoscale waves which were discussed in the previous sections depend very much on the ratio of day and night static stability. As it was pointed out earlier, it seems that, at least for a dry atmosphere, the boundary layer over land will be strongly unstable ($N_1^2/N_0^2 \approx 1$) and weakly unstable over the ocean ($N_1^2/N_0^2 \approx 0.5$). The increase of moisture content in the oceanic boundary layer, however, could be a compensating effect in making the oceanic boundary layer as unstable as the dryer boundary layer over land. Unfortunately, our simplistic model cannot differentiate land or ocean atmospheres. However, we will try to discuss the modification of the wave circulation when a characteristic moisture distribution is applied to the numerical model as modified to include condensation effects.

When moisture is included in the model, Eq. (3.8) for potential temperature as well as the equations for water vapor mixing ratio q and cloud water c become

$$\frac{\partial \theta}{\partial t} - \alpha_0 J(\psi,\theta) = \nabla \cdot \chi_e \nabla \theta + A[\bar{\theta}_i(z) - \bar{\theta}_i(3000)]\epsilon_D + \frac{L}{C_p \pi}\left[\frac{\partial q}{\partial t}\right], \quad (5.1)$$

$$\frac{\partial q}{\partial t} - \alpha_0 J(\psi,\theta) = \nabla \cdot \chi_e \nabla q - \left[\frac{\partial q}{\partial t}\right], \quad (5.2)$$

$$\frac{\partial c}{\partial t} - \alpha_0 J(\psi,\theta) = \nabla \cdot \chi_e \nabla c + \left[\frac{\partial q}{\partial t}\right], \quad (5.3)$$

where $[\partial q/\partial t]$ is the differential time derivative representing the rate at which water vapor is condensed to form cloud water. In the actual finite-difference equations, a one-iteration algorithm is used at each time step to predict the amount of water vapor, if any, which is to be condensed into or evaporated from cloud water in order to conserve total water content, while not exceeding the local saturation vapor pressure. [The method used for this particular model was obtained from Lipps[4] and is described in more detail by Ross and Orlanski (1975).]

Moisture can be introduced into the model in several different ways. One way is to assume an

[4] Personal communication.

initial distribution of water vapor and to run the model for the total duration of the previous solutions. However, this will be costly since the inclusion of moisture decreases the time step from 5 min to 1 min due to numerical stability considerations. In addition, no significant difference will occur between the dry and moist solutions until condensation occurs. A second possibility, and the one which we chose, is to start the moist run from a particular time step of the dry solution. Two consecutive days (13 and 14) were selected and each was run for 14 h starting from noon, a time of the day when the wave field is still weak. The initial relative humidity was chosen to be latitude-dependent, having a maximum at the equator (70%) and a minimum at the north and south boundaries (35%); the same variation was applied for the vertical dependence with a maximum at 2000 m and a minimum at the tropopause.

The streamfunction and relative humidity for three different times after noon of day 13 are shown (Moist I) in Fig. 19. For comparison, the dry solution for the streamfunction is also shown on the left side of the figure. The upper graphs at 1250 show only the initial conditions. Intensification of the cells can be noticed (middle graphs) at 9 h (2100) after the initiation of the run at a time which is 3 h after the maximum activity of the dry solution. The stippling in the lower part of the relative humidity graph indicates condensation. The cells become deeper and stronger due to the heat released by condensation. The lower graphs (0200 of day 14) of streamfunction (Moist I) show very deep cells located at the same positions where the dry cells were maximum. Notice that the latitudes for the strong convection are 6°S, 1°N and 10°N, with all of the other small cells that were present in the dry solutions being virtually eliminated.

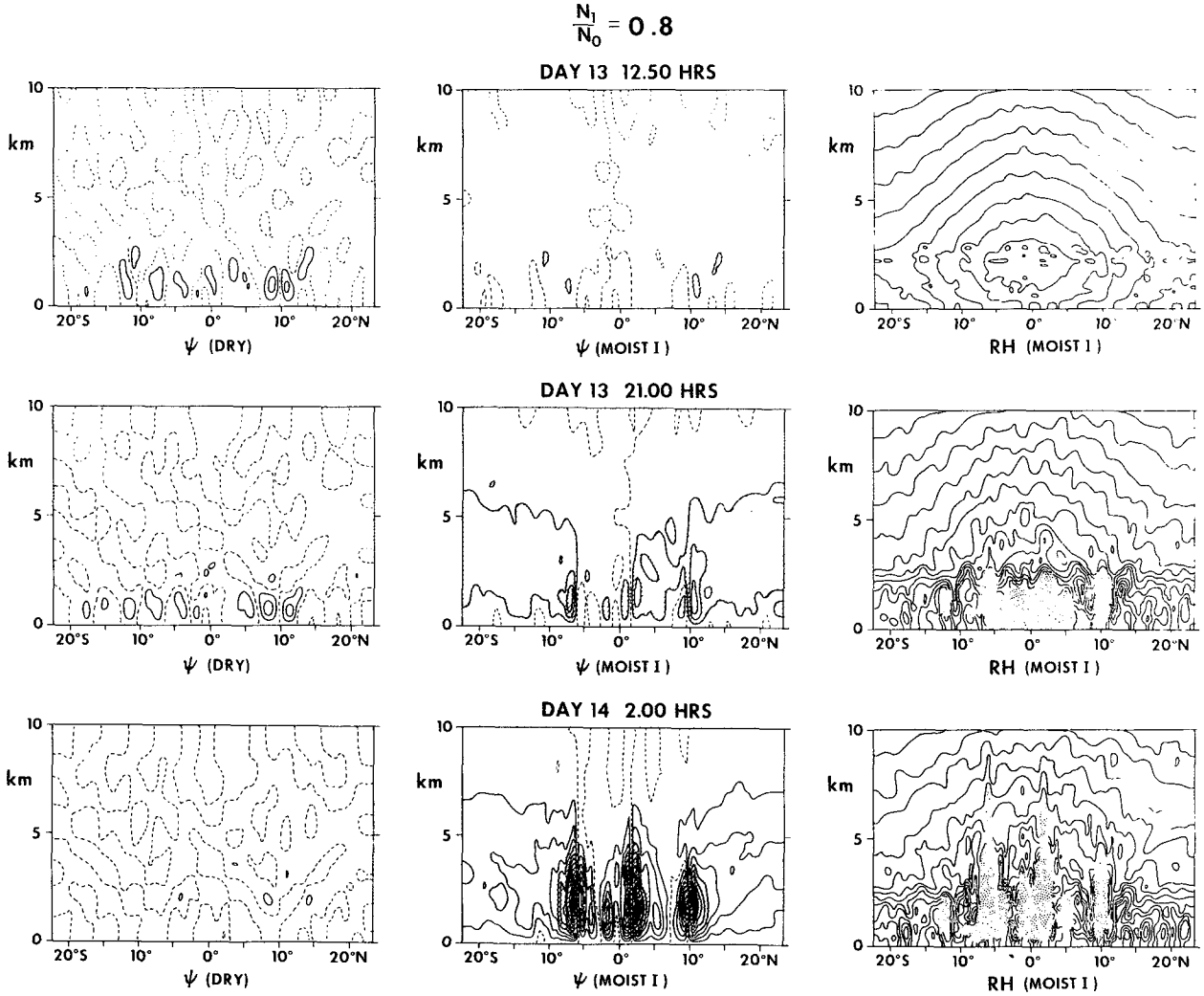

FIG. 19. Contours of streamfunction and relative humidity as a function of latitude and height at three times of the day for moist case I (see text). On the left the contours of streamfunction (dry) are shown for comparison.

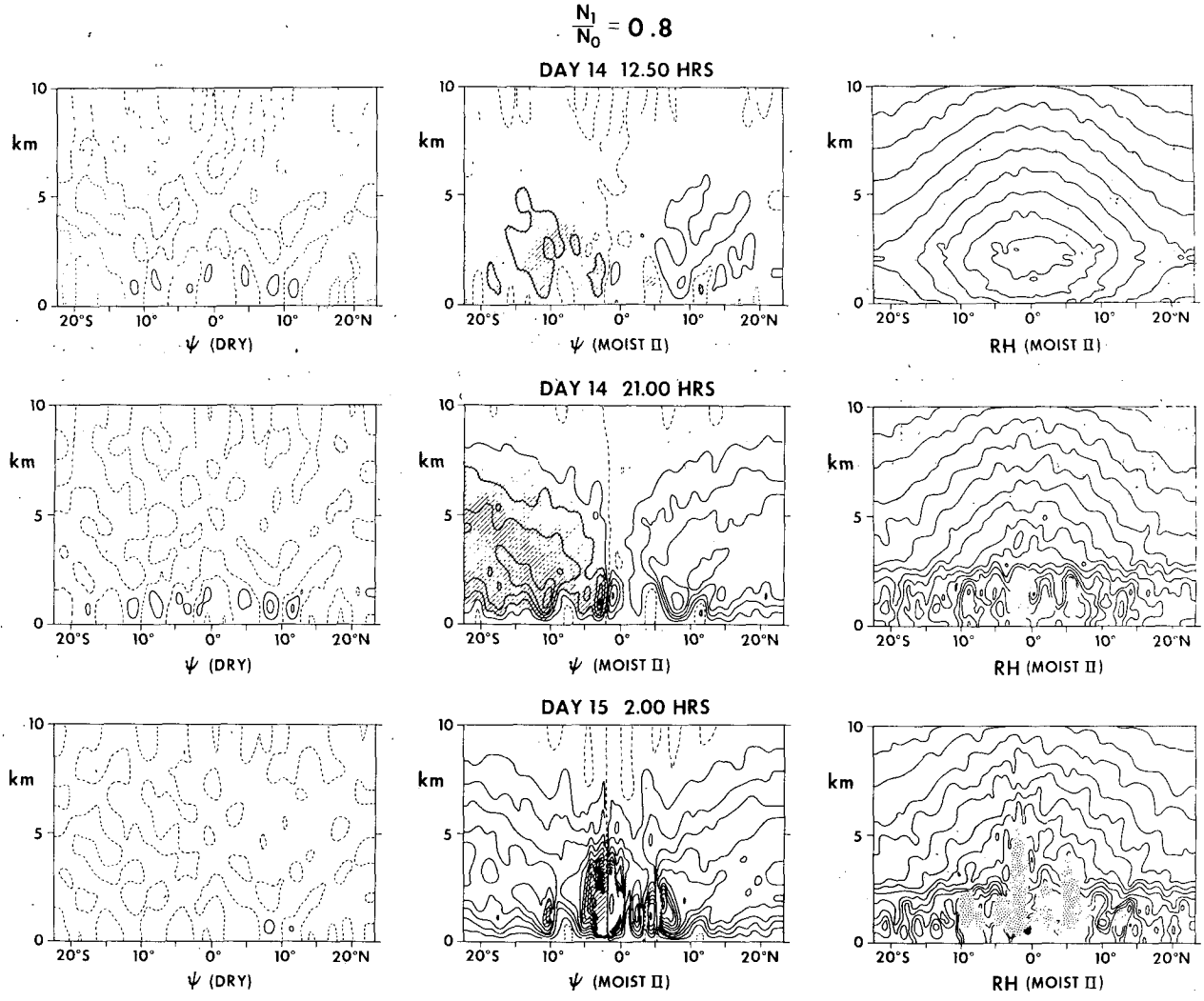

FIG. 20. As in Fig. 17 except for moist case II (see text).

Also note that deep columns of condensation in the relative humidity graph occur where the convective cells are present.

It would be unrealistic to continue this run much longer since no precipitation is allowed in our simplified scheme. However, the destabilizing effect of moisture for these waves is obviously apparent. As previously mentioned, in order to see the position of the deep convection for a consecutive day, a second run (Moist II) was started at 1200 of day 14. Graphs similar to those of Fig. 19 are shown in Fig. 20 for this case. We may notice, however, that although the intensification and general characteristics are the same as those of the previous day, the position of the deep cells changes to 2°S and 5°N, half the distance between the deep cells of the previous day. In fact, this is half the wavelength of the trapeze unstable waves, as was expected.

It should be pointed out that strong similarities are found between the numerical results and cloud systems over Africa, such as those shown in Fig. 5. The infrared pictures at night show patterns that alternate position for consecutive days in the same manner as those shown in the numerical solutions. Bearing in mind that the numerical model is very simple and has a strong limitation due to its two-dimensionality, we may conclude that the general characteristics and scales are well simulated.

The fact that deep convection occurs at around 10°N and 10°S and oscillates a few degrees each day as shown by the numerical solution, allows one to speculate that perhaps the trapeze instability mechanism is the cause for the observed oscillatory behavior which often occurs in the ITCZ. Such behavior has been reported by different scientists in the literature. To confirm this fact, more analyses of the observed position of the ITCZ are needed. Perhaps in future papers of the GATE observations, this point will be clarified.

6. Conclusions

A group of observational evidence concerning a 2-day periodicity in meteorological variables in the equatorial region has been presented and has led to the following conclusions:

1) A distinct 2-day peak is observed in the meridional wind component at different heights (surface, 850 mb, 700 mb).

2) The diurnal variability of temperature over the ocean is smaller than over land but is still significant for maintaining the trapeze instability mechanism.

3) The horizontal scales of cloud clusters are on the order of 400 km and their lifetime is about 1 day for these scales. Clusters over land are initiated during the early night hours.

4) A distinct 2-day peak was found in the total cloud cover frequency over the B array in the GATE area.

5) Alternative configurations of cloud patterns over Africa for consecutive days are revealed by satellite pictures which show maximum activity at night.

The numerical solution of a two-dimensional, β-plane equatorial model was investigated for a dry and a moist atmosphere, leading to the following conclusions:

1) The presence of a shear flow does not substantially modify the unstable trapeze waves, so long as the axes of the wave rolls are aligned parallel to the mean wind.

2) The β-effect slightly modifies the meridional structure of the inertia-gravity waves and has maximum activity in a 20° band centered at the equator.

3) The perpendicular (meridional in this model) horizontal wind component to the mean flow has a maximum amplitude for these 2-day waves.

4) The vertical and horizontal scales for these waves in the dry case are 2000 m and 800 km, respectively.

5) The upward motion in these waves produces deep convection in the presence of moisture and the location of the cells oscillates alternately from day to day.

From the above exposition of observational and numerical results, it seems reasonable to conclude that the diurnal variability in the equatorial atmosphere excites internal gravity waves in the form of mesoscale systems which are able to generate and control the cloud clusters that populate these areas.

Further work, both observational and theoretical, is needed for the complete evaluation of the effect of the so-called "diurnal tide" and the generation of mesoscale processes which are so important in the dynamics of the atmosphere, not merely at the equator but rather at all latitudes.

Acknowledgments. I would like to acknowledge Dr. Rodenhuis as well as Drs. Gruber and Replane for furnishing me with their unpublished data. I would also like to thank Dr. Bruce Ross and Dr. Y. Hayashi for reading the manuscript and for comments which helped to clarify the paper. Also, to Mr. Larry Polinsky for his valuable assistance in programming and analyzing the numerical results. In addition, I want to extend my thanks to Phil Tunison and Betty Williams for drafting the figures and typing the manuscript.

REFERENCES

Fels, S. B., 1974: The trapeze instability on an open domain. *J. Atmos. Sci.*, **30**, 434–443.

Gruber, A., and W. Replane, 1975: Preliminary analysis of GATE cloud and wind data. *Preprints 9th Tech. Conf. Hurricanes and Tropical Meteorology*, Key Biscayne, Fla., Amer. Meteor. Soc., 1–25.

Hayashi, Y., 1970: A theory of large-scale equatorial waves generated by condensation heat and accelerating the zonal wind. *J. Meteor. Soc. Japan*, **48**, 140–160.

——, 1974: Spectral analysis of tropical disturbances appearing in a GFDL general circulation model. *J. Atmos. Sci.*, **31**, 180–218.

Lindzen, R. S., 1974: Wave-CISK in the tropics. *J. Atmos. Sci.*, **31**, 156–179.

Lipps, F. B., 1970: Barotropic stability and tropical disturbances. *Mon. Wea. Rev.*, **98**, 122–131.

Martin, D. W., 1975: Characteristics of West African and Atlantic cloud clusters. GATE Rept. No. 14, Preliminary Scientific Results, Vol. 1, 182–190 [available from WMO, Geneva].

Matsuno, T., 1966: Quasi-geostrophic motions in the equatorial area. *J. Meteor. Soc. Japan*, **44**, 25–42.

McEwan, A. D., and R. M. Robinson, 1975: Parametric instability of internal gravity waves. *J. Fluid Mech.*, **67**, 667–688.

Murakami, M., 1972: Intermediate-scale disturbances appearing in the ITC Zone in the tropical western Pacific. *J. Meteor. Soc. Japan*, **50**, 454–464.

Nitta, T., 1972: Energy budget of wave disturbances over the Marshall Islands during the years of 1956 and 1958. *J. Meteor. Soc. Japan*, **50**, 71–84.

——, 1974: Diurnal variations in the western Atlantic trades during BOMEX. *J. Meteor. Soc. Japan*, **52**, 254–257.

Orlanski, I., 1973: Trapeze instability as a source of internal gravity waves, Part I. *J. Atmos. Sci.*, **30**, 1007–1016.

——, 1976: A simple boundary condition for unbounded hyperbolic flows. To be published.

——, B. B. Ross and L. J. Polinksy, 1974: Diurnal variation of the planetary boundary layer in a mesoscale model. *J. Atmos. Sci.*, **31**, 965–989.

Petrossiants, M. A., V. N. Ivanov, V. V. Galushko and J. A. Menshov, 1975: On characteristic time scales of meteorological fields in the tropical Atlantic zone. GATE Rept. No. 14, Preliminary Scientific Results, Vol. 2, 48–63 [available from WMO, Geneva].

Reed, R. J., and E. E. Recker, 1971: Structure and properties of synoptic-scale wave disturbances in the equatorial western Pacific. *J. Atmos. Sci.*, **28**, 1117–1133.

Ross, B. B., and I. Orlanski, 1975: Frontal dynamics (moist case). (Submitted to *J. Atmos. Sci.*)

Rotunno, R., 1975: Trapeze instability modified by a mean shear flow. (Submitted to *J. Atmos. Sci.*)

Thorpe, S. A., 1975: The excitation, dissipation, and interaction of internal waves in the deep ocean. *J. Geophys. Res.*, **80**, 328–338.

Yamasaki, M., 1969: Large-scale distrubances in the conditionally unstable atmosphere in low latitudes. *Pap. Meteor. Geophys.*, **20**, 289–336.

Yanai, M., 1963: A preliminary survey of large scale disturbances over the tropical Pacific region. *Geofis. Intern. (Mexico)*, **3**, 73–84.